

Setup and data analysis for functional magnetic resonance imaging of awake cat visual cortex

Manxiu Ma^{1,2}, Chencan Qian^{1,2}, Yanxia Li¹, Zhentao Zuo¹, Zuxiang Liu¹

¹State Key Laboratory of Brain and Cognitive Science, Institute of Biophysics, Chinese Academy of Sciences, Beijing 100101, China

²University of the Chinese Academy of Sciences, Beijing 100039, China

Corresponding author: Zuxiang Liu. E-mail: zxliu@bcslab.ibp.ac.cn

© Shanghai Institutes for Biological Sciences, CAS and Springer-Verlag Berlin Heidelberg 2013

ABSTRACT

Functional magnetic resonance imaging (fMRI) is one of the most commonly used methods in cognitive neuroscience on humans. In recent decades, fMRI has also been used in the awake monkey experiments to localize functional brain areas and to compare the functional differences between human and monkey brains. Several procedures and paradigms have been developed to maintain proper head fixation and to perform motion control training. In this study, we extended the application of fMRI to awake cats without training, receiving a flickering checkerboard visual stimulus projected to a screen in front of them in a block-design paradigm. We found that body movement-induced non-rigid motion introduced artifacts into the functional scans, especially those around the eye and neck. To correct for these artifacts, we developed two methods: one for general experimental design, and the other for studies of whether a checkerboard task could be used as a localizer to optimize the motion-correction parameters. The results demonstrated that, with proper animal fixation and motion correction procedures, it is possible to perform fMRI experiments with untrained awake cats.

Keywords: functional magnetic resonance imaging; cat; motion correction; non-rigid motion

INTRODUCTION

Functional magnetic resonance imaging (fMRI) provides extensive information on sensory, motor, and cognitive processing in humans. It has high spatial resolution and is noninvasive^[1,2]. Meanwhile, invasive methods such as microelectrode mapping, radioisotope tracing, and anatomical studies in animal models such as monkeys have greatly enhanced our knowledge about the function of the visual system^[3]. In recent decades, it has become increasingly important to combine MRI with invasive methods in animal studies. Structural MRI helps to guide or localize the placement of electrodes for single-cell recordings^[4-6] or to locate lesions^[7]. fMRI studies of anesthetized monkeys have been used to model visual areas without top-down influence^[8] and to localize the visual cortex^[9]. Awake monkey fMRI approaches have developed quickly and are widely used in cognitive neuroscience to functionally localize face areas^[10], to compare general sensory functions between humans and monkeys^[11,12], and to explore the functional mechanisms of neural signal propagation or intrinsic functional connectivity^[13].

Most of the studies scanning behaving monkeys have developed similar methods^[9,10,14-26]. One of the most important aspects in the awake monkey fMRI scan is to keep the monkey's head in position by invasively implanting a headpost on the skull or by noninvasive techniques, such as a vacuum helmet^[27]. Before scanning, the monkey must be trained to keep its body still during the experiment; such training is time-consuming and laborious.

Due to the difficulty of performing experiments, the number of monkey fMRI publications is relatively small compared with the number of human fMRI studies^[18]. Although it is possible to scan other primates, such as baboons^[28], a more promising approach is to enhance the power of animal fMRI to scan smaller animals^[29]. fMRI can be applied to rodents, songbirds, bats and fish^[30], and one recent study has advanced its application to awake rats using an 11.7-T scanner for the collection of resting-state data^[31]. However, these small animals require ultra-high-field scanners. As one of the most frequently-used animal models in vision studies^[32], the cat is more acceptable for awake fMRI studies because its brain is large enough to be studied using widely-available clinical human scanners. The first cat fMRI study was on anesthetized cats and demonstrated the blood oxygenation level-dependent (BOLD) response of visual area V2 to a drifting grating^[33]. Then, cat fMRI was used to map iso-orientation columns^[34], to perform fiber tracking^[35], and to study fiber development using diffusion spectrum imaging with a very high field^[36]. However, no fMRI study on awake cats has been reported because of the difficulties in restraining the cat to keep it motionless in the scanner and in training it in such a restrained condition. In general, cats are not as cooperative and focused^[37] as monkeys, which makes them more difficult to study in the awake state.

In the current study, we described the implementation of a setup for BOLD fMRI studies on awake cats using a clinical 3-Tesla scanner without animal training. There is evidence that without proper training, non-rigid movements of the jaw and body induce artifacts into the BOLD signals recorded from the brain^[20] due to fluctuations of the B0 field (the main magnetic field generated by the magnet). Motion-correction methods can help in the data analysis procedures; however, motion-correction algorithms sometimes introduce more artifacts under these conditions^[17]. Our setup helps to restrain cats but does not prevent them from performing non-rigid movements. In this study, we first demonstrated the BOLD responses of visual area V1 to a checkerboard stimulus with a standard motion-correction method, then described two approaches based on partial volume registration that can potentially be used to correct for non-rigid motion artifacts: a fast general approach that may apply to normal experimental design, and a sophisticated approach that requires the

checkerboard task as a localizer to optimize the parameters before its application to other cognitive processes, such as attention-related tasks.

METHODS

Animal Preparation

Four cats (3.2–4.4 kg, 2–3 years old, three male and one female, named CAT2 to CAT5) were used. All surgical and scanning procedures were performed under strictly aseptic conditions and were approved by the Committee on Animal Research at the Institute of Biophysics, Chinese Academy of Sciences. The cats were housed in separate cages (0.7 × 0.85 × 0.95 m³) designed for rhesus monkeys and fed cat food from a pet store.

Before the head-post implantation, the cats were initially intramuscularly (i.m.) injected with ketamine hydrochloride (20 mg/kg) and atropine (0.05 mg/kg), then maintained at surgical levels of anesthesia with 1–2% sodium pentobarbital (15 mg/kg, i.m.) for 2–3 h during the surgery. All implanted materials were tested for magnetic susceptibility prior to surgery. We chose ceramic screws and dental acrylic to implant a home-designed head-post made of polyether ether ketone (an advanced biomaterial used in medical implants) to restrain the animal's head (Fig. 1A). The post was affixed to the skull and extended vertically from the rostral cranium, similar to that used in alert monkey fMRI studies. Due to the relatively small size of the head, we used a rotate-and-lock design at the bottom surface of the head-post (see Fig. 1B for details) to embed the ceramic screws already fixed to the surface of the skull into the head post, and then we filled the gap with dental acrylic to firmly hold the head-post in place. Each cat was under intensive care for a week and then given a month of rest for recovery before the MRI scans. The animals were treated post-surgically with antibiotic (benzylpenicillin sodium, 10–12 mg/kg, i.m.) for 3 days. Wound margins on the skin surrounding the implant were cleaned with iodine and antibiotics every day after the surgery for 2 weeks until the wounds were no longer bleeding and the cats no longer scratched them.

Animal Chair

The cats were placed in the 'sphinx' position in an MRI-compatible primate chair during the scanning sessions. A

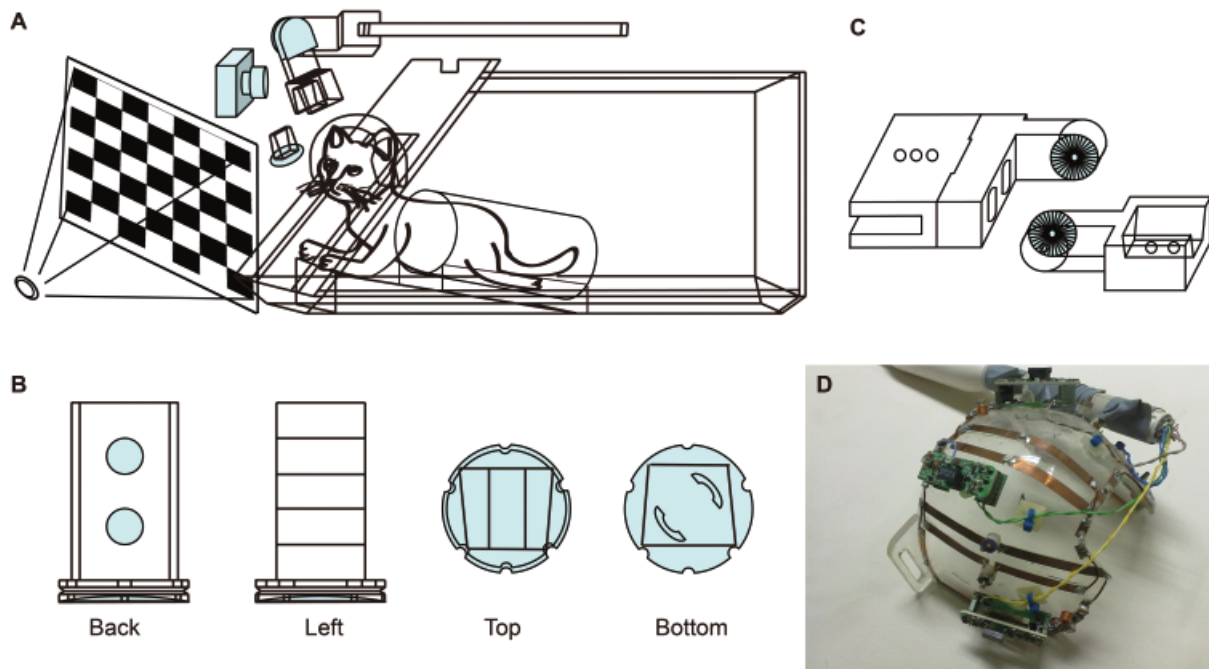


Fig. 1. A: Schematic drawing of the cat fMRI setup. The animal was placed in the sphinx position, and visual stimuli were presented from the front. The head was restrained by the implanted head post and the joint affixed to the animal chair. An MRI-compatible eye tracker was mounted in front of the right eye. **B:** Details of the head-post. Note the rotate-and-lock design in the bottom view. The head-post was implanted on the skull by ceramic screws and dental acrylic. **C:** Details of the joint. This design allowed three-dimensional adjustment and for the head-post to be implanted on either the anterior or posterior portion of the head, which made future neurophysiological recording more flexible. **D:** Photograph showing details of the custom-designed coil.

primate chair (from Massachusetts General Hospital) with an additional restrainer was used to hold the cats because they are smaller than average nonhuman primates. To prevent motion artifacts and to allow for more precise signal localization in the chair, we produced a nonmetallic apparatus to hold the cat's head in a fixed position during the fMRI scanning sessions. This was attached to the surgically-implanted cranial head-post. When the cat's head was in the fixed position, the head was oriented such that its face and eyes were directed toward a screen placed at the end of the horizontal bore of the magnet (Fig. 1A). No lens was used. We tested the setup on cats in our sham scanner with recorded scanning noise. Observations from the back of the projector confirmed that the cat kept its eyes open during the stimulus presentation. For CAT4 and CAT5, an MRI-compatible infra-red eye-tracker was mounted to the setup and captured real-time images of the eye.

An infrared camera on the wall at the foot end of the

scanner was used to monitor the cats. Although it was impossible to capture a clear view of the head with this camera because the distance between the scanner center and the camera was ~6 meters, and the view was blocked by the cat's body, it was easy to detect movements from a monitor in the console room if the cat moved its body or swung its tail.

Coil Details

A reception four-element surface coil array of almost equal sizes was built on an organic glass mold that covered the cat's head and was tuned to 123.2 MHz. Tuning and matching were achieved by a combination of the fixed and the adjustable capacitor. The switching of the receiver state was completed using a non-magnetic pin diode (DH80106). Coupling between adjacent elements was minimized by overlapping an appropriate geometric loop to reduce the mutual inductance. The coupling effect of further elements was neglected due to geometric distance

and low-impedance preamplifier decoupling. A balun was used to minimize cable decoupling. By measuring the scattering parameters, this coil design achieved a reflection coefficient for each element lower than -12 dB and the coupling coefficient measured between every element was below -15 dB (Fig. 1D). For CAT4 and CAT5, the coil was upgraded to a five-element design. The extra element was attached to the frontal part of the coil in order to increase the coverage of the frontal lobes of the brain.

Visual Stimuli

Visual stimuli were projected onto a screen at the end of the bore, 57 cm from the cat's eyes. A black-and-white checkerboard flickering at 2 Hz was presented in 5 blocks of 30 s active/30 s rest. Each session lasted 300 s, including 16 s of blank screen at the beginning, and each cat completed two scanning sessions.

MRI Protocols

Functional MRI was performed using a Siemens TIM 3T system (Siemens Medical Solutions, Erlangen, Germany). The built-in body coil was used for transmission and the home-made phase-array coil was used for reception. BOLD responses were acquired using single-shot gradient-echo echo-planar imaging (EPI) with the following parameters: field of view, 128 mm; repetition time (TR), 2000 ms; echo time (TE), 30 ms; flip angle, 90° ; matrix size, $64 \times 64 \times 25$; and voxel size, $2 \times 2 \times 2$ mm³. The functional scans consisted of 150 functional volumes while each volume

has 25 axial slices that covered the whole brain. A rapid anatomical scan that had the same center and slice orientation as the functional scans was obtained using a T1-weighted rapid three-dimensional gradient-echo (MP-RAGE) sequence with the following parameters: TR, 1520 ms; TE, 4.46 ms; flip angle, 15° ; voxel size, $0.5 \times 1 \times 0.5$ mm³; and 240 axial slices. An iso-resolution anatomical scan was obtained using the same MP-RAGE sequence with different parameters: TR, 1850 ms; TE, 4.85 ms; flip angle, 8° ; voxel size, $0.5 \times 0.5 \times 0.5$ mm³; and 176 sagittal slices. For CAT3, CAT4 and CAT5, an additional iso-resolution anatomical scan was obtained under anesthesia with the same parameters.

Eye-movement Monitoring

For CAT4 and CAT5, eye images were acquired by an MRI compatible infra-red eye-tracker (MRReyetracking from Resonance Technology Inc., Northridge, CA) mounted in front of the right eye through infra-red reflexive glass (Fig. 2A) at 60 Hz. The images were collected during the experiment and processed by ViewPoint (Arrington Research, Scottsdale, AZ). The position of the eye was indicated by the coordinates of the dark pupil center (Fig. 2B and C).

Data Analysis

Standard approach All pre-processing and analyses were performed with AFNI (<http://afni.nimh.nih.gov/afni/>) software. For the functional dataset, the acquired volumes

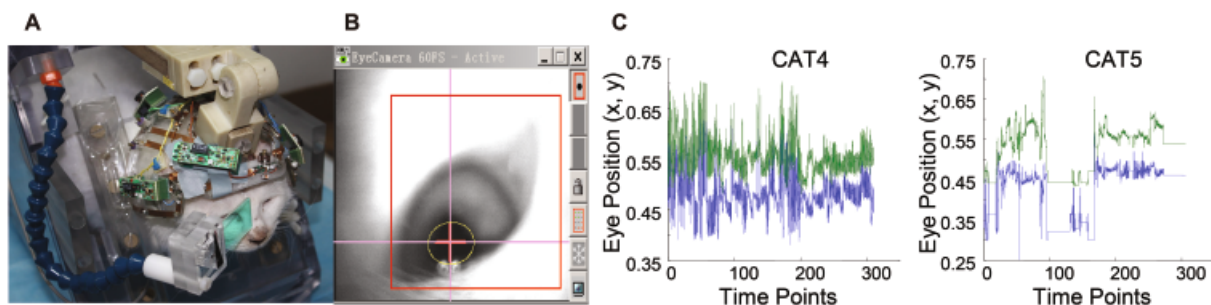


Fig. 2. Eye-movement monitoring devices and results. **A:** An MRI-compatible infra-red eye-tracker was mounted in front of the right eye using adjustable plastic tubes. A piece of infra-red reflexive glass projected the infra-red image of the eye to the camera while the cat could see the visible-light stimulus through it. **B:** A screenshot of the eye-tracking software. A region of interest was manually selected and labeled as a red rectangle. It was important to only include the eye. The dark pupil was automatically fit with a circle and the center of the circle was labeled as the crossing point. **C:** Eye position plots for CAT4 and CAT5 during an experiment. Blue curves indicate horizontal and green curves indicate vertical. Note that for CAT5 the curves showed flat periods. From real-time images as in (B), these indicated that the eye was closed.

were first corrected for slice timing. The timing-corrected data were registered to the third volume of the first run for motion-correction. The six motion parameters/profiles (left-right, anterior-posterior, up-down, pitch, roll and yaw) were generated. After spatial smoothing (Gaussian, FWHM 3 mm), the volumes were normalized to the mean intensity of each run on a voxel-by-voxel basis to obtain the percentage signal change (PSC). The data from the 2 runs were concatenated and subjected to multiple linear regression analysis. For the visual stimulation, regressors were generated by convolving a boxcar design matrix with a gamma function. The motion parameters from volume registration were put into the regression analysis

as regressors of no interest (Fig. 3, blocks linked by black arrows) and an activation map was obtained for the standard method.

For the anatomical dataset, the rapid anatomical scan and the high-resolution anatomical scan were aligned using the AFNI program '3dTagalign', by defining two markers at the bottom of each eye and one marker at the superior crossing of the tentorium cerebelli and longitudinal fissure. Because the rapid anatomical scan had a lower signal-to-noise ratio and less gray-white matter contrast, the functional results were aligned to and re-sampled with the high-resolution anatomical scan using the same tag settings as the rapid anatomical scan to generate activation

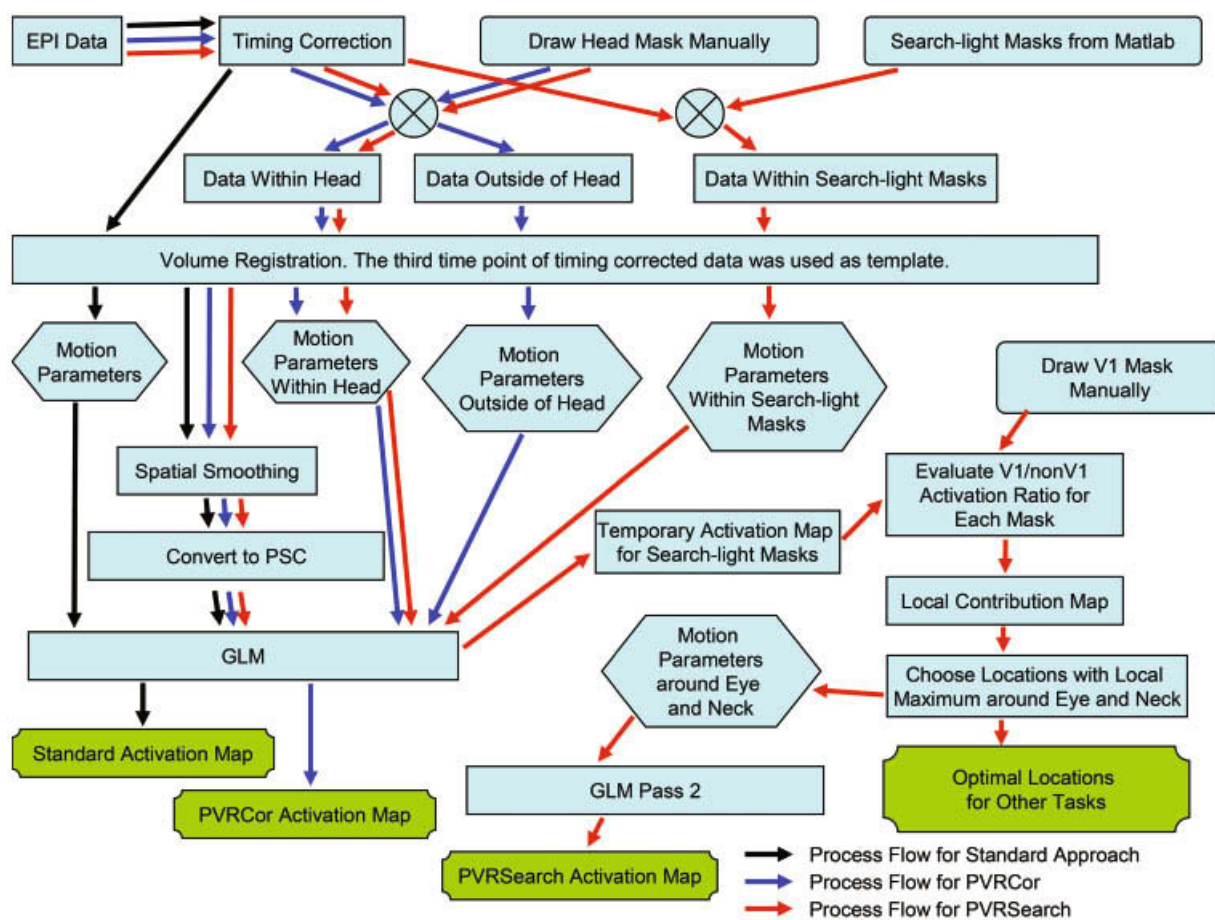


Fig. 3. Flowchart of the three processing methods. Processing steps are labeled as blue rectangles. Masks generated manually or by the Matlab toolbox are labeled as blue blocks with rounded corners. Blue circles with crosses indicate the combination of information from different resources to generate one or two output datasets. Motion parameters generated by volume registration are labeled as blue hexagons. Final activation maps or best parameters selected are labeled as green blocks. The process flow for the standard method is indicated by black arrows. The PVRCor process flow is indicated by blue arrows and the PVRSearch process flow by red arrows.

maps. For CAT3 to CAT5, the high-resolution anatomical scan obtained under anesthesia was used.

Partial volume registration correction (PVRCor) Partial volume registration means registering part of the EPI data to the timing-corrected dataset. PVRCor is a fast general approach to correct for non-rigid motion artifacts facilitated by partial volume registration.

The fast anatomical scan session had the same center and orientation of slices as the EPI scan sessions. A head mask was created manually from the fast anatomical scan for each cat. In this head mask, the brain, skull and scalp were included, while the jaw, eyes and neck were excluded.

For the functional dataset, the acquired volumes were first corrected for slice timing. The timing-corrected data were masked by the head mask: the signals within the mask were retained and the signals outside of the mask were set to zero. A non-head dataset was also derived from the head mask: the signals within the mask were set to zero and the signals outside of the mask were unchanged. So the timing-corrected data were split into two datasets by the headmask: data within the head and data outside of the head (Fig. 3, blue arrows). Both datasets were aligned to the third volume of the timing-corrected data, and motion parameters for both datasets were generated. After spatial smoothing (Gaussian, FWHM 3 mm), the data within the head were normalized to the mean intensity of each run on a voxel-by-voxel basis to obtain the PSC. The data from the 2 runs were concatenated and subjected to multiple linear regression analysis. For the visual stimulation, regressors were generated by convolving a boxcar design matrix with a gamma function. The motion parameters from both datasets were used in the regression analysis as regressors of no interest (Fig. 3, blocks linked by blue arrows) and an activation map was obtained for the PVRCor method.

ROI and index definition In spite of the head mask, a visual area V1 mask was defined based on the anatomical details^[38] of each cat. In addition, a brain mask was defined from the anatomical data. A non-V1 brain mask was obtained by subtracting the V1 mask from the brain mask. Before applying the masks to the EPI data, the head mask, the V1 mask and the non-V1 brain mask were re-sampled to $2 \times 2 \times 2$ mm resolution.

To quantify the activation map, mean t values were

calculated using the defined V1 and non-V1 brain masks. The ratio of the values between the V1 mask and the non-V1 brain mask, defined as the index of the ratio of activation ($t_{V1}/(t_{V1}+t_{non-V1})$), measured the sensitivity of the procedure to detect activation evoked by the visual stimulus.

Partial volume registration with search-light (PVRSearch) In this approach, a search-light paradigm was used. For each possible location in the EPI data space, a mask centered at this location was created (mask size, $11 \times 11 \times 11$ voxels) by the AFNI Matlab toolbox. A total of 43740 ($54 \times 54 \times 15$) search-light masks were generated.

For the functional dataset, the acquired volumes were first corrected for slice timing. The timing-corrected data were masked by the head mask and the data within the head were obtained. The dataset was registered to the third volume of the timing-corrected data and motion parameters were generated. After spatial smoothing (Gaussian, FWHM 3 mm), the data within the head were normalized to the mean intensity of each run on a voxel-by-voxel basis to obtain the PSC. The data from the 2 runs were concatenated and subjected to multiple linear regression analysis. For the visual stimulation, regressors were generated by convolving a boxcar design matrix with a gamma function.

For each possible location in the EPI data space, a masked dataset was generated from the timing-corrected data and its corresponding search-light mask. This search-light masked dataset was aligned to the third volume of the timing-corrected data, and motion parameters were collected. The motion parameters from the within-head dataset and the search-light masked dataset were put into the regression analysis as regressors of no interest and a temporary activation map was generated. The V1 *versus* non-V1 activation ratio was calculated from the temporary activation map for this location. The activation ratios from all locations were combined into a local contribution map. Locations with a local maximum (one near the eye and one near the neck, in most cases) were selected by manually inspecting the local contribution map. The motion parameters from these two locations, in addition to the motion parameters from the within-head dataset, were put into the regression analysis as regressors of no interest and a final activation map was obtained for the PVRSearch method (Fig. 3, blocks linked by red arrows). These two

locations with a local maximum could be applied to other tasks scanned in the same configuration.

RESULTS

For CAT4 and CAT5, eye movements in the MRI scanner during the experiment were monitored by the eye-tracker. The images of the right eye were captured in real time by ViewPoint (Fig. 2B). CAT4 kept its eyes open throughout the experiment, with some eye movements revealed by the exported coordinates of eye position. CAT5 sometimes closed its eyes during the experiment, resulting in flat lines in the eye-position plot (Fig. 2C). We noted that fitting the cat pupil with a circle is not as precise as in human subjects since its shape changed to oval at the beginning of each block with the flickering checkerboard.

The setup and coil proved to be reliable. EPI images showed a good signal-to-noise ratio. However, the voxel intensity near the headpost was lower than that inside the brain (Fig. 4A). The BOLD signal changed with stimulus on-off in visual areas such as V1, with fluctuations that could not be explained by the experimental design. The signal changes in the eye and neck area had amplitudes similar with that in V1, indicating large local motion artifacts, which were not directly associated with the stimulus paradigm (Fig. 4B).

The local contribution maps from all cats had common patterns. We found that two areas in CAT2, one at the neck and one above the left eye, made the largest contribution to the correction for activation ratio. In CAT3, the largest values were located at the neck, in deep brain areas, in visual areas, and near the eyeball. In both CAT4 and CAT5, a local maximum near the right eye and a local maximum at the neck were found (Fig. 5A). To demonstrate the relationship between these local maxima, the motion parameters generated with masks located at the ROIs of CAT3 and the whole brain are shown in Figure 5B. The motion parameters showed that the pattern of eyeball ROI was different from the others or the whole brain. The ventral brain ROI and the neck ROI had opposite patterns in the yaw direction and shared a similar pattern in the anterior-posterior direction, indicating body-induced artifacts. In spite of that, the V1 ROI showed a combined influence from the eyeball ROI and the neck ROI.

The activation maps generated by the standard

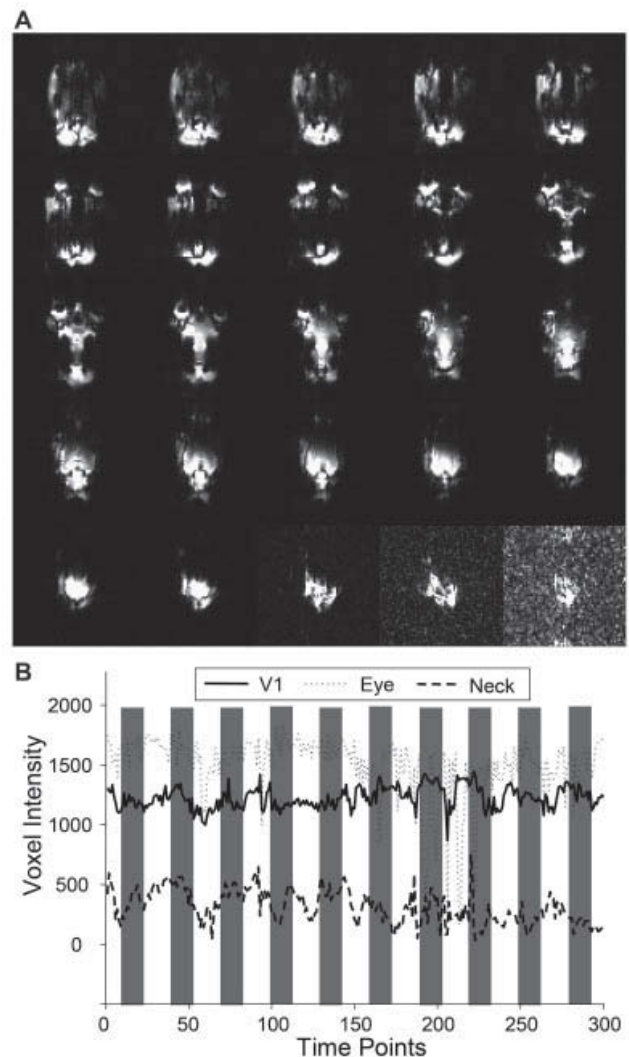


Fig. 4. Raw EPI data collected from the setup. **A:** Each image shows a slice of the EPI dataset, from one time point in the functional data from CAT2. Note the low voxel intensity at the very top of the brain, due to the influence of the headpost, ceramic screws and dental acrylic. **B:** Time-courses from voxels at different locations. The gray bars indicate the presentation of the flickering checkerboard. The voxel in V1 showed responses to the on-off the visual stimulus, with artifacts that were not correlated with the stimulus paradigm. The signals in voxels at the eye and neck changed with the same or even larger amplitude than that of the V1 voxel.

method, PVRCor and PVRSearch are shown in Figure 6. The V1 masks for each cat are also shown. It is clear that with a checkerboard stimulus, there were activations in the visual area and other brain or non-brain areas when

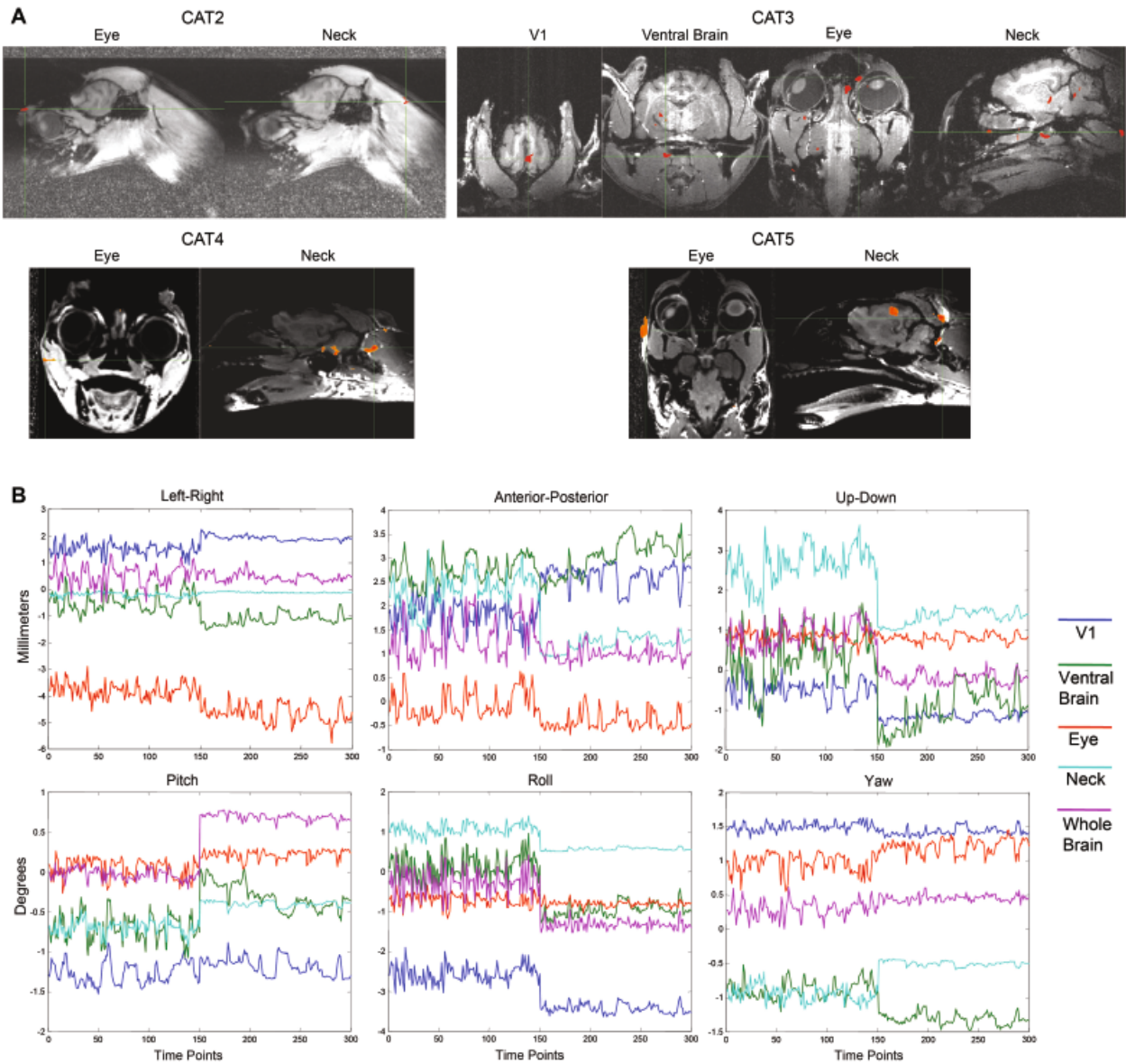


Fig. 5. Results of the search-light paradigm. A: Each image shows a location where motion information contributed most to the improvement of the V1 *versus* non-V1 index in activation maps. In CAT2, one location was above the left eye and one at the neck. In CAT3, the locations were at the left eye, deep brain, neck, and occipital area. In CAT4 and CAT5, one location was near the right eye and one at the neck. **B:** Motion parameters from CAT3 generated with masks located at V1, ventral brain, eye, neck, and the brain mask. Translations are in millimeters and rotations in degrees relative to the third volume of the first scan. The motion parameters demonstrated: first, the motion pattern of the eyeball ROI was different from the others or the whole brain; second, the ventral brain and the neck ROIs had opposite patterns in the yaw direction and shared a similar pattern in the anterior-posterior direction, indicating body-induced artifacts; and third, the V1 ROI showed a combined influence from the eyeball ROI and the neck ROI.

the data were processed by the standard method. With the PVRCor method, the pattern was more stable with fewer activations outside the brain and outside of V1. The activation ratio increased from 96.43% to 96.85% in CAT2,

60.87% to 90.59% in CAT3, and 18.99% to 36.65% in CAT4. In CAT5, the activation ratio dropped slightly from 60.93% to 52.49% (Table 1). In any case, the activation maps showed that the activations in the cerebellum were

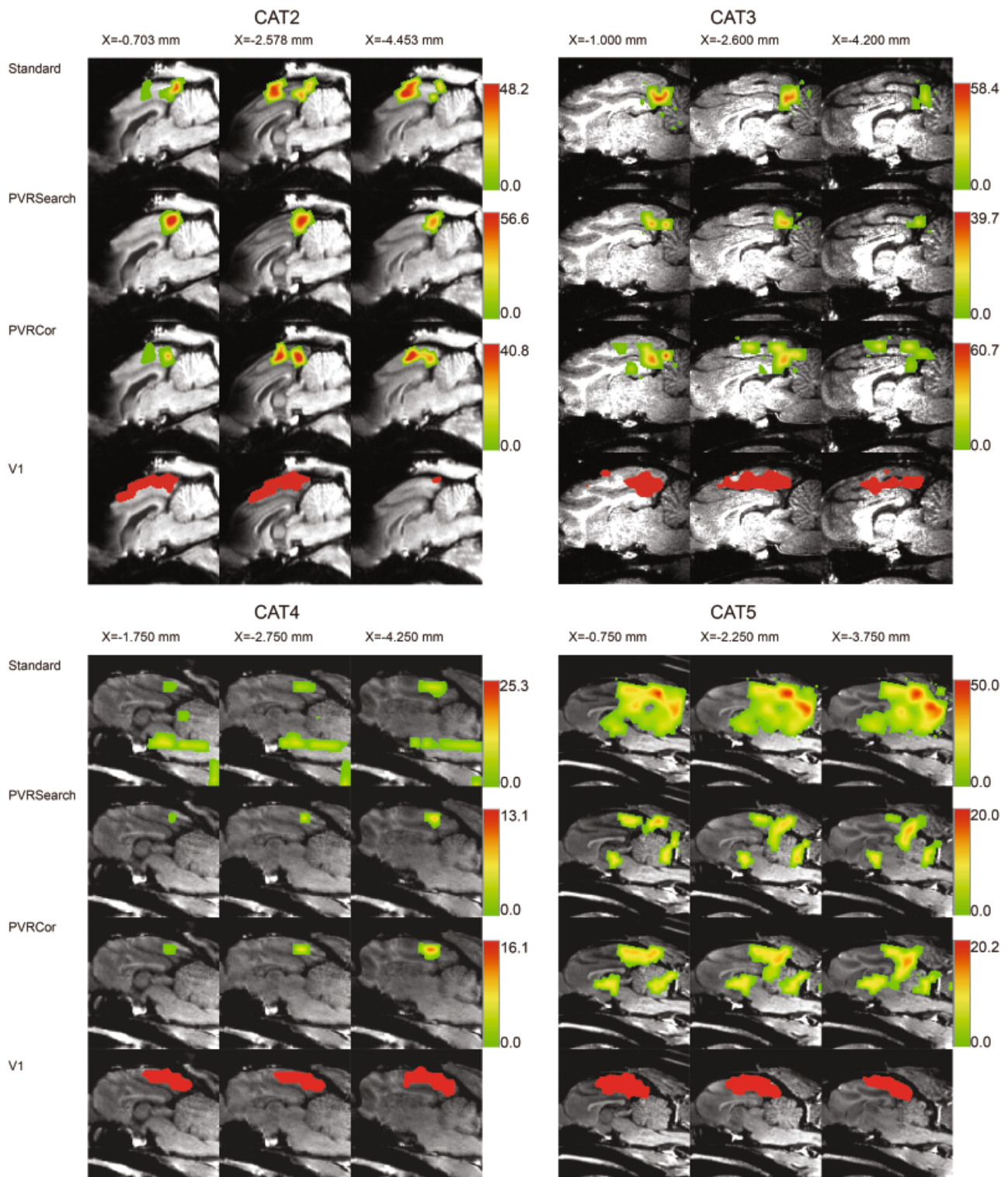


Fig. 6. BOLD fMRI activation responses to the checkerboard stimulus. Different motion correction procedures are shown in different rows. Color bars indicate F values. Note that the standard method detected activations within and outside V1. The PVRCor method gave a cleaner pattern, with less activation outside V1. The PVRSearch corrected activations outside V1 and increased the signal in V1.

Table 1. Comparison of different motion-correction procedures in four cats

		Mean activation in V1	Mean activation in brain areas outside V1	Mean activation ratio (%)
CAT2	Standard	7.57	0.28	96.43
	PVRCor	4.30	0.14	96.85
	PVRSearch	9.03	0.17	98.15
CAT3	Standard	0.42	0.27	60.87
	PVRCor	10.40	1.08	90.59
	PVRSearch	4.62	0.03	99.37
CAT4	Standard	0.19	0.79	18.99
	PVRCor	0.07	0.15	36.65
	PVRSearch	0.17	0.06	71.64
CAT5	Standard	8.12	5.21	60.93
	PVRCor	0.97	0.87	52.49
	PVRSearch	2.86	0.84	77.35

PVRCor: motion-correction with partial volume registration and motion-correction based on information from a non-head mask; PVRSearch: motion-correction with partial volume registration, combined with the best data points from a search-light algorithm for external motion information; Standard: standard motion-correction procedure.

largely removed by PVRCor in CAT5. When the motion parameters were optimized by PVRSearch, the activation was stronger in the visual area, as suggested by increased activation ratios from 96.85% to 98.15% in CAT2, 90.59% to 99.37% in CAT3, 36.65% to 71.64% in CAT4 and 52.49% to 77.35% in CAT5.

The PVRSearch approach not only increased the activation ratio, which was the direct result of the selection of local maxima in the local contribution map, but also decreased the residual errors in general linear regression analysis (Fig. 7). The residual error test showed that, compared with the standard method, the best combination of motion profiles significantly decreased the residual errors [for CAT2, $t(299) = 6.096$, $P < 0.001$; for CAT3, $t(299) = 6.074$, $P < 0.001$; for CAT4, $t(299) = 3.714$, $P < 0.001$; and for CAT5, $t(299) = 7.910$, $P < 0.001$]. These results suggested that the superior performance of the PVRSearch method was not because of the particular optimization of the index, defined as the ratio of activation in the V1 mask area and non-V1 brain areas, which was solely in the spatial domain; the PVRSearch method also helped to explain the variance across volumes at the voxel level in the time domain.

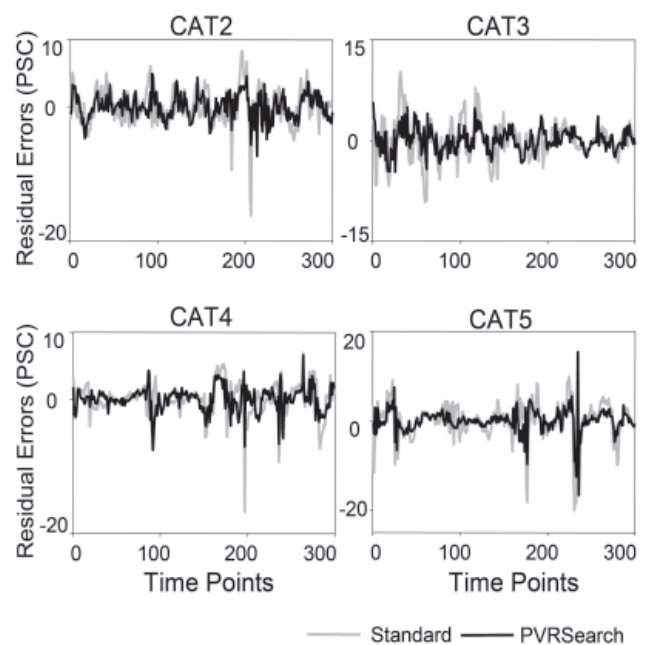


Fig. 7. Comparison of residual errors between the standard method and PVRSearch. It is clear from the time-courses that PVRSearch had fewer residual errors, indicating that the search-light paradigm and PVRSearch were not only optimized to enhance the responses in V1 or the index we defined but also improved the results in the time domain.

DISCUSSION

In this study, we described the use of fMRI in awake cats. We introduced a setup adapted from monkey fMRI and the modified design of a headpost to fit cats. Our custom-made phase-array coil performed reliably in this configuration. We found that body movement-induced non-rigid motion introduced artifacts into the functional scans, especially those around the eye and neck. To correct for these artifacts, we developed two methods: PVRCor, for general experimental design, and PVRSearch, for studies of whether a checkerboard task could be used as a localizer to optimize the motion-correction parameters.

Head fixation and motion control are important issues that must be addressed for successful fMRI studies in the awake monkey^[14]. An MRI-compatible head-post implanted on the skull is the most commonly used device for head fixation^[9,15,17-24,26]. Although noninvasive methods have been proposed for monkey studies^[27], a plastic head-post is still the best choice if we are to extend fMRI experiments to cats, due to the complexity of the noninvasive methods. There is little risk of knocking the head-post off because of the relatively small body-size and strength of a cat. However, the cat head is smaller and the space for a head-post is limited. The rotate-and-lock design on the bottom surface of the head post can hold two extra screws, by which the skull area underneath the head-post was used to strengthen the implantation. Our results showed that even with the standard motion-correction method, significant activations were found in visual areas.

Despite the head fixation, artifacts induced by the movement of other parts of the body or head must be carefully examined. It has previously been shown that limb and torso movements induce B0 fluctuations, resulting in spatial distortion^[17]. To reduce jaw and body movement-induced artifacts in the fMRI time series, a novel training paradigm that allows monkeys to move their body between trials has proven successful^[20]. However, it may take 6 months to train a monkey to remain still in the scanner^[39], and even longer for the animal to adapt to more sophisticated motion-control paradigms. It is unknown how much time would be required to train small animals, such as the cat, to achieve similar motion-control performance. In the current study, we demonstrated that movements of several components of the head and neck significantly

influenced the BOLD signal. More than that, we found that eyeball movements may induce artifacts into visual areas, which was not found in previous monkey tests^[20], but is consistent with some human studies^[40,41]. A possible difference between our experiment and the tasks used in monkey studies is that monkeys were at least required to look at the fixation point for a period of time, while in our experiment the cats were in a pure free-viewing condition.

In our setup, an eye-tracker mounted in front of the eye allowed us to monitor the eye position and whether the cat remained awake during the experiment. However, we found several issues that must be noted. In the cat, the pupil changes its shape to oval when the luminance of the environment changes. The eye-tracking software fit the dark pupil with a circle, so the eye position was not as accurate as in human subjects. A possible solution is to design the visual stimulus such that no significant luminance change is involved. For example, a static checkerboard, instead of a blank screen, may be used to contrast with a flickering checkerboard in this experiment. Another problem of using this eye-tracker for cats is that the color of the hair around the eye must be considered. It is assumed by the software that only the pupil is dark. For a cat with dark hair around the eye (CAT4 in our experiment), even after carefully choosing the ROI, the system may fit the circle to dark hair near the eye and give wrong results, especially when the pupil shrinks to a very small size. We suggest using cats with white hair to avoid this problem.

The motion-correction methods we developed demonstrated that, even without motion-control training, it was possible to achieve reliable fMRI activation by proper correction for non-rigid motion induced by movements of head components or the body. The power of motion-correction in fMRI has been tested in apparent physiological noise-induced motion, especially respiratory fluctuations^[31]. Although several motion-correction methods have been proposed for various applications, e.g., boundary-based registration^[42], nonlinear deformation algorithms^[43], special registration algorithms, spatial deformation consideration and tensor orientation for diffusion tensor images^[44], motion correction for cardiac and head motion artifacts in diffusion-weighted images^[45], and multi-manifold diffeomorphic matrix mapping^[46], the difference between these and our method is that we factored the motion information outside of the brain area into a regression analysis of the brain activation.

Researchers have previously demonstrated three problems that post-processing motion-correction cannot resolve: insufficient volume coverage, signal variations, and local volumetric distortions by B0 inhomogeneity^[47]. In their study, they tracked the movement of the phantom and adjusted the slice position in real time during the acquisition, and then they used the motion parameters to generate a B0 field-inhomogeneity map. Finally, they corrected the distortion combined with the motion-correction and field map. The B0 field inhomogeneity and distortion were not directly corrected in our method, but signal variations induced indirectly by motion were considered in the form of local motion-correction parameters. The advantages of our method are that it is easy, fast, and can be achieved using most of the popular fMRI analysis tools, such as AFNI and SPM. However, combining our method with the B0 inhomogeneity correction paradigm^[47] and a novel real-time motion-detection method using a self-encoded marker^[48] would be optimal; macroscopic field inhomogeneity^[49] and motion artifacts could be estimated in k-space rather than in image domains^[50].

Easily reared and widely available, the cat is one of the most frequently-used animal models^[32] and has helped to advance our understanding of the development of the visual system^[51], the effects of lesions^[52,53], and the mechanisms of perceptual learning^[37]. Behavior tests from those studies involved using a nose-operated key, which is prohibited in the MRI environment because of head fixation. Cats can also be trained to do behavioral responses by the paw^[54,55], but our data suggest that movements of body parts other than the head also induced artifacts into the fMRI time series, which means the paw response test is not an ideal choice. Biophysical and single-neuron studies^[56,57] have demonstrated that it is possible to train awake cats to respond using eye movements during cognitive tasks, similar to monkey studies. However, as revealed in our data, eye movements should be carefully evaluated since they also introduce artifacts into the BOLD signal. A possible solution is keeping the eyeball away from the coverage of the functional scans with proper slice positioning^[40,41]. It is also important to note that we recorded eye movements in image coordinates. Our eye-tracker has the option to export the eye-movement information in stimulus space as visual angles, if calibrated. However, to calibrate the eye-tracker, our eye-tracking software requires

the subject to keep and shift fixations to 9 sequentially-presented squares on the screen, which is very unlikely for a cat. We believe that a better solution is to calibrate the eye-tracker in each experiment only when necessary, using a reflexive saccade stimulus, which is commonly used in monkey behavioral training.

The limitation of the current study is that the sensitivity index we used (V1 *versus* non-V1 ratio) assumed that our visual stimulus did not activate brain areas outside of V1. This assumption is not necessarily correct, especially when the cat is under restraint and stressed. However, the index improvement found by including the non-rigid motion information in our analysis showed that even if activations outside of V1 were evoked, motion artifacts also contributed to the activation patterns. We believe the motion artifacts influenced the BOLD signal in a task-relevant way, in which V1 and non-V1 signals were corrected differently by the included motion profiles, resulting in an increase of the index. It is also true that the V1 mask generated manually for each cat was very subjective and that the ROI definition was very specific to the visual experiment. However, for the general version, PVRCor, the improvement of activation detection did not rely on the definition of V1, even though the same index measure was used. More importantly, this index helped us to achieve the best parameters from PVRsearch. We believe this is especially useful for localizer experiments, such as face-selective patches. A general approach to study the response properties of face-selective patches is to localize them in a localizer experiment, with different categories of pictures or scrambled pictures, including faces. After that, other experiments are done to evaluate the responses of those ROIs to, for example, inverted faces. In this sense, PVRsearch could be implemented based on a localizer experiment, to find the best combinations that optimize the response of face-selective patches. Then the best combination, though it may vary between animals, could be applied to other experiments, regarding the amplitude of the response in the localizer experiment as a common reference. In our study, the checkerboard task could be used as a localizer experiment to get optimized parameters, then applying them to other, for example, attention tasks.

Although it may not be easy to train cats in tasks with a high cognitive load, similar to the work that has been performed in some monkey studies, the cat is

more widely available and is a good candidate for fMRI experiments, especially for those combining fMRI with microstimulation^[13], microinjection^[58], pharmacological MRI combined with electrophysiology^[59], or reversible deactivation with a cooling system^[60]. Our setup and motion-correction method represent critical first steps toward successful fMRI investigation in the awake cat. We believe our methods, with the help of fMRI as a functional localizer, have tremendous potential for extending our understanding of the functional architecture of the cat visual system and exploring cognition in the nervous system in general.

ACKNOWLEDGEMENTS

This work was supported by grants from the Ministry of Science and Technology of China (2012CB825500, 2012IM030100, 2010IM030800), and the National Natural Science Foundation of China (91132302, 90820307). We thank Zhu Huabing for advice on coil design, Robert Desimone, Daniel Baldauf and Kang Cheng for helpful comments on the manuscript.

Received date: 2012-08-14; Accepted date: 2013-02-17

REFERENCES

- [1] Heeger DJ, Ress D. What does fMRI tell us about neuronal activity? *Nat Rev Neurosci* 2002, 3: 142–151.
- [2] Op de Beeck HP, Haushofer J, Kanwisher NG. Interpreting fMRI data: maps, modules and dimensions. *Nat Rev Neurosci* 2008, 9: 123–135.
- [3] Nassi JJ, Callaway EM. Parallel processing strategies of the primate visual system. *Nat Rev Neurosci* 2009, 10: 360–372.
- [4] Fujimichi R, Naya Y, Koyano KW, Takeda M, Takeuchi D, Miyashita Y. Unitized representation of paired objects in area 35 of the macaque perirhinal cortex. *Eur J Neurosci* 2010, 32: 659–667.
- [5] Matsui T, Koyano KW, Koyama M, Nakahara K, Takeda M, Ohashi Y, *et al.* MRI-based localization of electrophysiological recording sites within the cerebral cortex at single-voxel accuracy. *Nat Methods* 2007, 4: 161–168.
- [6] Scherberger H, Fineman I, Musallam S, Dubowitz DJ, Bernheim KA, Pesaran B, *et al.* Magnetic resonance image-guided implantation of chronic recording electrodes in the macaque intraparietal sulcus. *J Neurosci Methods* 2003, 130: 1–8.
- [7] Moore T, Rodman HR, Repp AB, Gross CG, Mezrich RS. Greater residual vision in monkeys after striate cortex damage in infancy. *J Neurophysiol* 1996, 76: 3928–3933.
- [8] Rainer G, Augath M, Trinath T, Logothetis NK. Nonmonotonic noise tuning of BOLD fMRI signal to natural images in the visual cortex of the anesthetized monkey. *Curr Biol* 2001, 11: 846–854.
- [9] Logothetis NK, Guggenberger H, Peled S, Pauls J. Functional imaging of the monkey brain. *Nat Neurosci* 1999, 2: 555–562.
- [10] Tsao DY, Freiwald WA, Knutsen TA, Mandeville JB, Tootell RB. Faces and objects in macaque cerebral cortex. *Nat Neurosci* 2003, 6: 989–995.
- [11] Koyama M, Hasegawa I, Osada T, Adachi Y, Nakahara K, Miyashita Y. Functional magnetic resonance imaging of macaque monkeys performing visually guided saccade tasks: comparison of cortical eye fields with humans. *Neuron* 2004, 41: 795–807.
- [12] Nakahara K, Hayashi T, Konishi S, Miyashita Y. Functional MRI of macaque monkeys performing a cognitive set-shifting task. *Science* 2002, 295: 1532–1536.
- [13] Matsui T, Tamura K, Koyano KW, Takeuchi D, Adachi Y, Osada T, *et al.* Direct comparison of spontaneous functional connectivity and effective connectivity measured by intracortical microstimulation: An fMRI study in macaque monkeys. *Cereb Cortex* 2011, 21(10): 2348–2356.
- [14] Andersen AH, Zhang Z, Barber T, Rayens WS, Zhang J, Grondin R, *et al.* Functional MRI studies in awake rhesus monkeys: methodological and analytical strategies. *J Neurosci Methods* 2002, 118: 141–152.
- [15] Dubowitz DJ, Chen DY, Atkinson DJ, Grieve KL, Gillikin B, Bradley WG Jr, *et al.* Functional magnetic resonance imaging in macaque cortex. *Neuroreport* 1998, 9: 2213–2218.
- [16] Durand JB, Nelissen K, Joly O, Wardak C, Todd JT, Norman JF, *et al.* Anterior regions of monkey parietal cortex process visual 3D shape. *Neuron* 2007, 55: 493–505.
- [17] Gamlin PD, Ward MK, Bolding MS, Grossmann JK, Twieg DB. Developing functional magnetic resonance imaging techniques for alert macaque monkeys. *Methods* 2006, 38: 210–220.
- [18] Goense JB, Whittingstall K, Logothetis NK. Functional magnetic resonance imaging of awake behaving macaques. *Methods* 2010, 50: 178–188.
- [19] Hadj-Bouziane F, Bell AH, Knutsen TA, Ungerleider LG, Tootell RB. Perception of emotional expressions is independent of face selectivity in monkey inferior temporal cortex. *Proc Natl Acad Sci U S A* 2008, 105: 5591–5596.
- [20] Keliris GA, Shmuel A, Ku SP, Pfeuffer J, Oeltermann A, Steudel T, *et al.* Robust controlled functional MRI in alert monkeys at high magnetic field: effects of jaw and body movements. *Neuroimage* 2007, 36: 550–570.
- [21] Maier A, Wilke M, Aura C, Zhu C, Ye FQ, Leopold DA. Divergence of fMRI and neural signals in V1 during

- perceptual suppression in the awake monkey. *Nat Neurosci* 2008, 11: 1193–1200.
- [22] Peeters R, Simone L, Nelissen K, Fabbri-Destro M, Vanduffel W, Rizzolatti G, *et al.* The representation of tool use in humans and monkeys: common and uniquely human features. *J Neurosci* 2009, 29: 11523–11539.
- [23] Pinski MA, Moore T, Richter MC, Gross CG, Kastner S. Methods for functional magnetic resonance imaging in normal and lesioned behaving monkeys. *J Neurosci Methods* 2005, 143: 179–195.
- [24] Stefanacci L, Reber P, Costanza J, Wong E, Buxton R, Zola S, *et al.* fMRI of monkey visual cortex. *Neuron* 1998, 20: 1051–1057.
- [25] Tsao DY, Vanduffel W, Sasaki Y, Fize D, Knutsen TA, Mandeville JB, *et al.* Stereopsis activates V3A and caudal intraparietal areas in macaques and humans. *Neuron* 2003, 39: 555–568.
- [26] Vanduffel W, Fize D, Mandeville JB, Nelissen K, Van Hecke P, Rosen BR, *et al.* Visual motion processing investigated using contrast agent-enhanced fMRI in awake behaving monkeys. *Neuron* 2001, 32: 565–577.
- [27] Srihasam K, Sullivan K, Savage T, Livingstone MS. Noninvasive functional MRI in alert monkeys. *Neuroimage* 2010, 51: 267–273.
- [28] Wey HY, Li J, Szabo CA, Fox PT, Leland MM, Jones L, *et al.* BOLD fMRI of visual and somatosensory-motor stimulations in baboons. *Neuroimage* 2010, 52: 1420–1427.
- [29] Van der Linden A, Van Camp N, Ramos-Cabrera P, Hoehn M. Current status of functional MRI on small animals: application to physiology, pathophysiology, and cognition. *NMR Biomed* 2007, 20: 522–545.
- [30] Hu K, Li Y, Gu X, Lei H, Zhang S. Brain structures of echolocating and nonecholocating bats, derived *in vivo* from magnetic resonance images. *Neuroreport* 2006, 17: 1743–1746.
- [31] Kalthoff D, Seehafer JU, Po C, Wiedermann D, Hoehn M. Functional connectivity in the rat at 11.7T: Impact of physiological noise in resting state fMRI. *Neuroimage* 2011, 54: 2828–2839.
- [32] Kayser C, Salazar RF, Konig P. Responses to natural scenes in cat V1. *J Neurophysiol* 2003, 90: 1910–1920.
- [33] Jezzard P, Rauschecker JP, Malonek D. An *in vivo* model for functional MRI in cat visual cortex. *Magn Reson Med* 1997, 38: 699–705.
- [34] Kim DS, Duong TQ, Kim SG. High-resolution mapping of iso-orientation columns by fMRI. *Nat Neurosci* 2000, 3: 164–169.
- [35] Kim DS, Kim M, Ronen I, Formisano E, Kim KH, Ugurbil K, *et al.* *In vivo* mapping of functional domains and axonal connectivity in cat visual cortex using magnetic resonance imaging. *Magn Reson Imaging* 2003, 21: 1131–1140.
- [36] Takahashi E, Dai G, Wang R, Ohki K, Rosen GD, Galaburda AM, *et al.* Development of cerebral fiber pathways in cats revealed by diffusion spectrum imaging. *Neuroimage* 2010, 49: 1231–1240.
- [37] Hua T, Bao P, Huang CB, Wang Z, Xu J, Zhou Y, *et al.* Perceptual learning improves contrast sensitivity of V1 neurons in cats. *Curr Biol* 2010, 20: 887–894.
- [38] Tusa RJ, Rosenquist AC, Palmer LA. Retinotopic organization of areas 18 and 19 in the cat. *J Comp Neurol* 1979, 185: 657–678.
- [39] Dubowitz DJ, Chen DY, Atkinson DJ, Scadeng M, Martinez A, Andersen MB, *et al.* Direct comparison of visual cortex activation in human and non-human primates using functional magnetic resonance imaging. *J Neurosci Methods* 2001, 107: 71–80.
- [40] Chen W, Zhu XH. Suppression of physiological eye movement artifacts in functional MRI using slab presaturation. *Magn Reson Med* 1997, 38: 546–550.
- [41] Zhang X, Ross TJ, Salmeron BJ, Yang S, Yang Y, Stein EA. Single subject task-related BOLD signal artifact in a real-time fMRI feedback paradigm. *Hum Brain Mapp* 2011, 32: 592–600.
- [42] Greve DN, Fischl B. Accurate and robust brain image alignment using boundary-based registration. *Neuroimage* 2009, 48: 63–72.
- [43] Klein A, Andersson J, Ardekani BA, Ashburner J, Avants B, Chiang MC, *et al.* Evaluation of 14 nonlinear deformation algorithms applied to human brain MRI registration. *Neuroimage* 2009, 46: 786–802.
- [44] Xue Z, Li H, Guo L, Wong ST. A local fast marching-based diffusion tensor image registration algorithm by simultaneously considering spatial deformation and tensor orientation. *Neuroimage* 2010, 52: 119–130.
- [45] Zwiers MP. Patching cardiac and head motion artefacts in diffusion-weighted images. *Neuroimage* 2010, 53: 565–575.
- [46] Zhong J, Qiu A. Multi-manifold diffeomorphic metric mapping for aligning cortical hemispheric surfaces. *Neuroimage* 2010, 49: 355–365.
- [47] Boegle R, Maclaren J, Zaitsev M. Combining prospective motion correction and distortion correction for EPI: towards a comprehensive correction of motion and susceptibility-induced artifacts. *MAGMA* 2010, 23: 263–273.
- [48] Forman C, Aksoy M, Hornegger J, Bammer R. Self-encoded marker for optical prospective head motion correction in MRI. *Med Image Comput Assist Interv* 2010, 13: 259–266.
- [49] Meng Y, Lei H. A single-scan T2* mapping method based on two gradient-echo images with compensation for macroscopic field inhomogeneity. *Magn Reson Med* 2008, 60: 1388–1395.
- [50] Costagli M, Waggoner RA, Ueno K, Tanaka K, Cheng K.

- Correction of 3D rigid body motion in fMRI time series by independent estimation of rotational and translational effects in k-space. *Neuroimage* 2009, 45: 749–757.
- [51] Pasternak T, Movshon JA, Merigan WH. Creation of direction selectivity in adult strobe-reared cats. *Nature* 1981, 292: 834–836.
- [52] Orban GA, Vandenbussche E, Sprague JM, De Weerd P. Orientation discrimination in the cat: a distributed function. *Proc Natl Acad Sci U S A* 1990, 87: 1134–1138.
- [53] Rudolph KK, Pasternak T. Lesions in cat lateral suprasylvian cortex affect the perception of complex motion. *Cereb Cortex* 1996, 6: 814–822.
- [54] May BJ, Sachs MB. Dynamic range of neural rate responses in the ventral cochlear nucleus of awake cats. *J Neurophysiol* 1992, 68: 1589–1602.
- [55] Roelfsema PR, Engel AK, Konig P, Singer W. Visuomotor integration is associated with zero time-lag synchronization among cortical areas. *Nature* 1997, 385: 157–161.
- [56] Kang I, Malpeli JG. Dim-light sensitivity of cells in the awake cat's lateral geniculate and medial interlaminar nuclei: a correlation with behavior. *J Neurophysiol* 2009, 102: 841–852.
- [57] Kang I, Reem RE, Kaczmarowski AL, Malpeli JG. Contrast sensitivity of cats and humans in scotopic and mesopic conditions. *J Neurophysiol* 2009, 102: 831–840.
- [58] Logothetis NK, Augath M, Murayama Y, Rauch A, Sultan F, Goense J, *et al.* The effects of electrical microstimulation on cortical signal propagation. *Nat Neurosci* 2010, 13: 1283–1291.
- [59] Rauch A, Rainer G, Augath M, Oeltermann A, Logothetis NK. Pharmacological MRI combined with electrophysiology in non-human primates: effects of Lidocaine on primary visual cortex. *Neuroimage* 2008, 40: 590–600.
- [60] Khachaturian MH, Arsenault J, Ekstrom LB, Tuch DS, Vanduffel W. Focal reversible deactivation of cerebral metabolism affects water diffusion. *Magn Reson Med* 2008, 60: 1178–1189.